

Design, Fabrication, and Characterization of a Single-Aperture 1.5-MHz/3-MHz Dual-Frequency HIFU Transducer

Jianguo Ma, Sijia Guo, Di Wu, Xuecang Geng, and Xiaoning Jiang

Abstract—High-intensity focused ultrasound (HIFU) treatment efficiency is critical in maximizing the hyperthermia and reducing the surgery time. In this paper, a single-aperture, 1.5 MHz/3 MHz dual-frequency HIFU transducer was designed, fabricated, and characterized for tissue ablation enhancement. Double PZT-2 layers were configured in serial and dual-frequency ultrasound waves can be concurrently generated by exciting one of the PZT-2 layers. Impulse responses from the prototype showed that the wave amplitudes at 1.5 and 3 MHz were about the same, and both are more than 12 dB larger than those of higher orders of harmonics. Tissue ablation tests demonstrated that higher temperature rise can be achieved with dual-frequency ultrasound than with single-frequency ablation at the same acoustic power.

I. INTRODUCTION

THE first experimental use of high-intensity focused ultrasound (HIFU) was proposed in 1942, by ablating tissue inside with little harm on the surface [1]. Since then, HIFU has become an important tool for noninvasive therapy [2]–[6]. In general, HIFU therapy induced the hyperthermia effect, which was used to clinically manage a broad range of cancer and benign maladies [7], including solid tumors [8], [9], breast tumors [10], blood–brain barrier [11], [12], and prostate cancer [13].

To increase the ablation efficiency of HIFU treatment, multi-frequency ultrasound has been studied in recent years by a few groups [14]–[18]. As an example, the dual frequency tissue ablation experiments were carried out by simultaneously irradiating porcine liver regions of interest with confocal ultrasound transducers at 1.563 and 1.573 MHz [14], where the frequency difference is 10 kHz. It was found that dual-frequency HIFU induced larger lesions than conventional single-frequency HIFU under the same power density, which was likely a result of enhanced cavitation.

Cavitation is a controversial effect in HIFU ablation, which is classified into stable and inertial cavitation. Of the two, inertial cavitation bubbles generate broadband noise, which could reradiate the incident sound and thus enhance heat generation, the scheme of which makes major contributions to heating enhancement [19]. Research shows that cavitation-induced heating could generate a few times greater heat deposition than that induced by ultrasound only, largely because of the enhancement of cavitation yield from multi-frequency ultrasound [15]–[18], [20], [21]. It was also found that a three-beam configuration could further increase cavitation yield (a combination of 28 kHz, 1 MHz, and 1.66 MHz) [22]. In a quantitative comparison of single- and multi-frequency HIFU ablation, temperature rise showed that the ablation efficiency of multi-frequency ultrasound is higher than that of single-frequency ultrasound [23]. Treatment with dual-frequency exposure showed better effect on prolonging life of tumor-bearing-mice [24]. Besides enhanced heating, cavitation also aids monitoring of the location of the heat deposition [19].

Multi-frequency ultrasound takes advantage of cavitation, but, in many cases, increases the complexity and cost of the HIFU system. For example, the focal zones of the multiple transducers must overlap one another so as to generate enhanced inertial cavitation. Multiple transducers must be driven by multiple amplifiers and multiple function generators, which is prohibitive in implementing a HIFU array system with a large number of elements [23], [25]. An initial effort into exciting a HIFU transducer with harmonic signals was explored to create high efficiency at low complexity [17], [26]. However, resonance of higher harmonics was weak compared with the base frequency resonance.

In this study, a single-aperture, dual-frequency HIFU transducer was designed and fabricated with identical focal point for both working frequencies. First, performance of the multilayer resonator design was analyzed, and design parameters were optimized with Krimholtz–Leedom–Mattaiei (KLM) modeling [27] and the Field II program [28]. Then, the two-layer, dual-frequency transducer was fabricated and characterized. Finally, a tissue ablation test was performed using the prototype transducer and the same driving electronic equipment in both single-frequency and dual-frequency modes for ablation efficiency comparison.

Manuscript received January 12, 2013; accepted May 4, 2013. This project was supported under a University of North Carolina Translational and Clinical Sciences (TRaCS) pilot grant (#50KR71106).

J. Ma, S. Guo, D. Wu, and X. Jiang are with the Department of Mechanical & Aerospace Engineering, North Carolina State University, Raleigh, NC (e-mail: xjiang5@ncsu.edu).

X. Geng is with Blatek Inc., State College, PA.

D. Wu is also with Beijing Jiaotong University, Beijing, China.

DOI <http://dx.doi.org/10.1109/TUFFC.2013.2724>

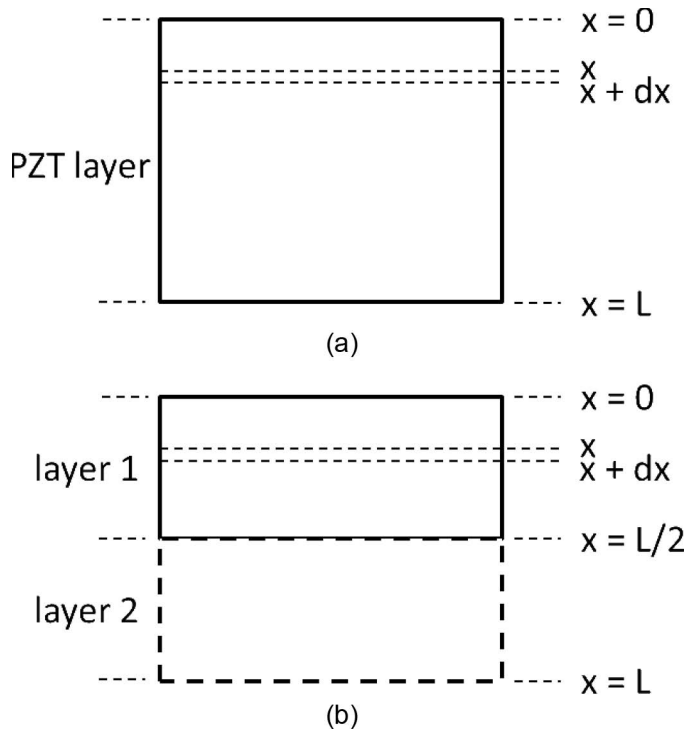


Fig. 1. Configuration of (a) single-layer and (b) double-layer transducers.

II. DESIGN METHOD AND SIMULATION

A. Single-Layer Resonator

A piezoelectric transducer is basically a vibrating plate [single layer, Fig. 1(a)], the motion of which is defined as the wave propagation equation

$$u(x, t) = Ae^{j(\omega t - kx)} + Be^{j(\omega t + kx)}. \quad (1)$$

For the ideal case of an ultrasound transducer with little load, the front surface and back surface are considered as being free to move, which means there is no force, and thus no strain, at either surface [29]. Symmetry of a homogeneous piezoelectric plate determined that only odd orders of harmonics exist [30]. Therefore, the vibration mode becomes

$$u_n(x, t) = \tilde{A}_n \cos\left(\frac{n\pi x}{L}\right) e^{j\omega_n t}, \quad (n = 1, 3, 5, \dots), \quad (2)$$

where L is the thickness of the piezoelectric material and $\omega_n = (n\pi c)/L$, with n indicating the n th vibration mode (as shown in Fig. 2).

With matching layer and backing layer added to the transducer, the front and back surfaces are not necessarily free to move, resulting in a frequency shift in each mode. Transmission line analysis provides a better approximation [31]. However, the ideal case (free-free vibration mode) provides a basic guideline for the transducer design.

For a homogenous piezoelectric plate, the amplitude of higher order harmonics, such as third and fifth harmonic, are pretty low (< -12 dB for this transducer) for a HIFU transducer because of the narrow bandwidth in most cases, and the relative strength of each harmonic is hardly tunable. As a result, transducers with a single homogenous piezoelectric layer are not widely used to generate dual or multiple frequencies in HIFU ultrasound.

B. Double-Layer Resonator

To design a single-aperture dual-frequency transducer, the overall piezoelectric material is divided into two identical layers, as shown in Fig. 1(b). With this configuration, only layer 1 of the transducer is excited, while layer 2 of the transducer acts as a backing layer. Because the thickness is halved, twice the initial frequency is generated. Instead of staying still, the plane at the center of the transducer vibrates, introducing vibration modes of $\omega'_n = (2n\pi c)/L$, where values with a prime indicate the double-layer transducer. As shown in Fig. 3, the frequency of each order of harmonic introduced by the double-layer tran-

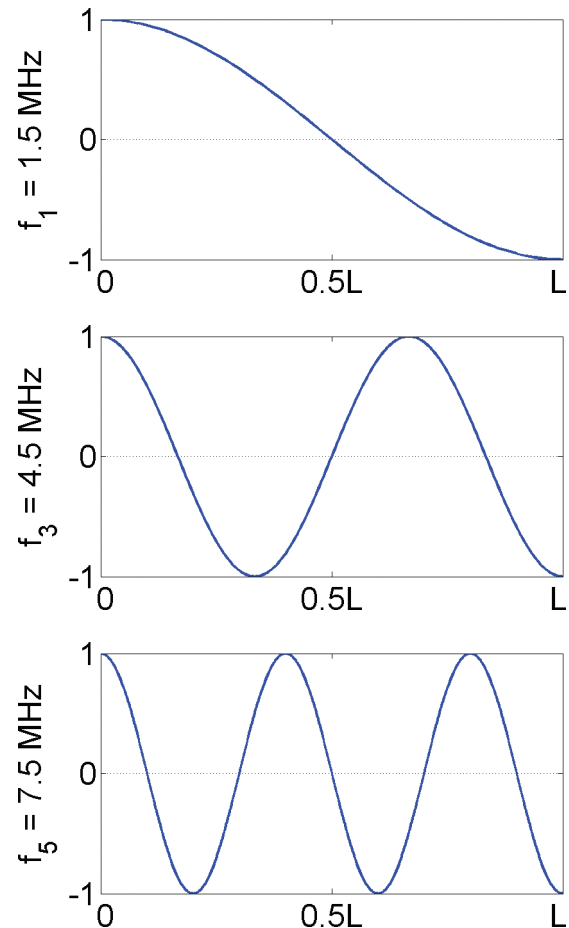


Fig. 2. Vibration modes of a single-layer transducer. Values on y -axis indicate the relative displacement in each mode. L is the thickness of the active (piezo) material.

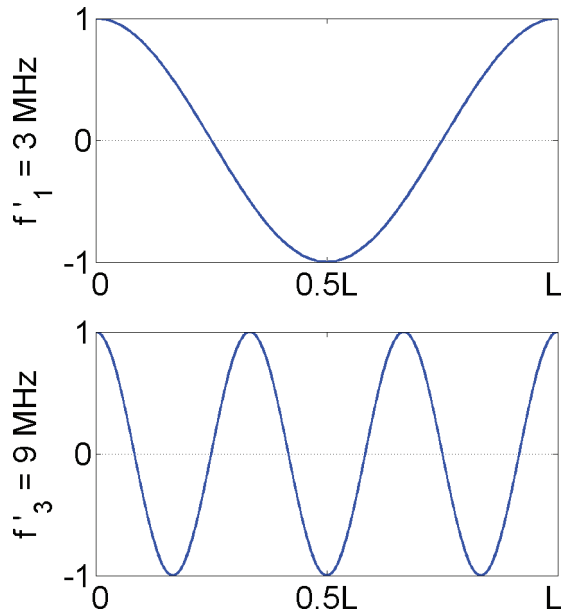


Fig. 3. Additional vibration modes of a double-layer transducer. Values on y -axis indicate the relative displacement in each mode. L is the total thickness of 2-layer piezo material.

ducer is twice that of the single-layer transducer ($\omega'_n = 2\omega_n$). At base frequency with $n = 1$, both ω_n and ω'_n meet the requirements of the boundary condition. As a result, dual-frequency ultrasound can be generated with this single-aperture transducer.

Compared with a single-layer transducer with the same overall thickness, a dual-layer transducer introduces another group of vibration modes (ω'_n), which is twice the frequency (ω_n) of the single-layer transducer. With proper design, i.e., thickness of active layers and matching layer, base frequencies at the two groups could be adjusted to be close to each other. At the same time, amplitude of the two base frequencies is still much larger (>12 dB) than that of higher order harmonics.

C. Transducer Configuration

Based on the analysis, a dual-layer, dual-frequency, single-aperture transducer was designed as shown in Fig. 4. Two layers of PZT-2 were mechanically bonded together and electrically controlled separately so that the transducer could vibrate at different modes. Mechanically, two PZT-2 layers were bonded in series. If the front layer vibrates, the back layer acts as a backing layer; in the other case, in which the back layer vibrates, the front layer acts

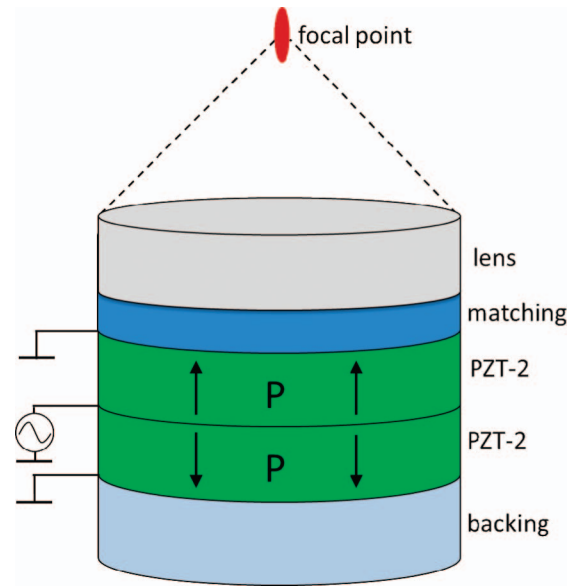


Fig. 4. Configuration of the dual frequency transducer. Arrows on the transducer around “P” indicate the polarization direction.

as a matching layer. The thickness of each PZT-2 layer is one-half the wavelength of a 3 MHz ultrasound wave, so that the resonant frequency for each PZT-2 layer is 3 MHz. Bonded together, the two PZT-2 layers could vibrate as one layer with twice the thickness and vibrate at the same mode, yielding 1.5 MHz ultrasound. In this case, the dual-frequency transducer could work in 3-MHz mode or 1.5-MHz mode. The polarization of the two PZT-2 layers is opposite. In electrical view, electrodes between the two layers are shorted as a firing signal. The front electrode of the front layer and the back electrode of the back layer could be grounded together, or one grounded while the other is left unconnected. Thus, choices are available by exciting one layer or both layers. A summary of the vibration modes is listed in Table I.

D. KLM Modeling

The goal of this transducer design was to obtain dual-frequency ultrasound with similar acoustic pressures from a single aperture. The KLM model was used to estimate the performance of the transducer. In particular, the electrical impedance spectra of single-layer and double-layer resonators were modeled considering different matching and backing materials.

In the modeling, 1.5- and 3-MHz configurations were simulated separately. For the modeling of the 1.5-MHz

TABLE I. SUMMARY OF VIBRATION MODES OF THE TRANSDUCER.

	Front-layer excitation	Dual-layer excitation
Electrical view	1 layer excited	2 layers in parallel connection
Mechanical view	Active layer with backing	Homogeneous active layer
Resonant mode(s)	3 MHz and 1.5 MHz	1.5 MHz

TABLE II. MATERIAL PARAMETERS OF THE LAYERS OF THE PROTOTYPED TRANSDUCER.

	Back support	Active	Matching
Material	Hard air	PZT-2	Graphite
Shape	Round	Round	Round
Diameter (mm)	25.4	25.4	25.4
Thickness (mm)	NA	0.735	0.172
Sound speed (m/s)	NA	4430	3230
Impedance (MRayl)	0.5	34.1	6.0
Relative dielectric constant	NA	560	NA
Coupling coefficient kt	NA	0.52	NA
Mechanical quality factor	NA	1000	NA
Dielectric loss	NA	0.002	NA

single-frequency configuration, the two PZT-2 layers were considered as one thick layer. With this assumption, the transmitting electrical impedance should be a quarter of the simulated value because of the mechanical serial, electrical parallel configuration. For the 3-MHz configuration, the front PZT-2 layer was used as the active layer and the back one was considered as the backing layer.

Because there are two frequency modes in the transducer, the quarter-wavelength matching layer could match only one frequency. Attenuation is higher in materials at higher frequency, so the matching layer was set to match the 3-MHz transducer to balance the power output of the two frequencies. Based on KLM simulation, thickness of the matching layer was set to be 0.16λ for 3 MHz ultrasound.

E. Acoustic Field Simulation

In HIFU applications, targets beneath the skin are exposed to high pressure while keeping the surface of the skin little affected. The key is to keep the acoustic pressure at the skin within a low level and to focus ultrasound at target to achieve a pressure high enough to induce the hyperthermia effect, thus damaging the tumor or cancer cells; therefore, it is essential to evaluate the acoustic field distribution.

Field II [28], a Matlab-based toolkit (Matlab, The MathWorks Inc., Natick, MA), was used to perform the field simulation. The surface of the transducer is concave because a lens was added to the transducer. The focal length of the transducer is 15 mm. A concave model was used in the simulation with a radius of 12.7 mm and focal radius of 15 mm. A continuous wave was supplied to the transducer with an effective voltage of 100 V, corresponding to 283 Vpp. Based on KLM modeling, pressures generated by the transducer were 2.85 and 1.81 kPa/V for 1.5 and 3 MHz ultrasound, respectively. Because the transducer is axially symmetric, the emitted field was simulated with Field II on the y - z plane, with the z -axis being the axial direction of the transducer. The boundary was set as -15 mm to 15 mm in the y -direction and 0 mm to 40 mm in the z -direction to well cover the area of interest.

III. FABRICATION AND CHARACTERIZATION

A. Fabrication

PZT-2, a piezoelectric ceramic material from the Shanghai Ceramic Institute, was used as the active material in the transducer. PZT-2 plates with resonant frequency of 3 MHz were prepared with the thickness of 0.735 mm and diameter of 25.4 mm. Two such pieces of PZT-2 ceramic plate were bonded together with epoxy, forming the dual-frequency transducer. It was verified that the thickness of the epoxy bonding layer was less than 5 μm . Compared with the thickness of the PZT layers (735 μm), such a thin bonding layer was considered to be negligible for the vibration at the designed frequencies. In the wave forwarding direction, a block of graphite, 7.825 mm in thickness, was bonded to the surface of the PZT-2 ceramic. The graphite block was then machined to form a 15-mm-radius curvature with 7 mm depth of curvature. In the backing direction, a very lossy microbubble-filled epoxy, known as hard air, with an acoustic impedance of 0.5 MRayl was bonded to the PZT-2 back surface to support the piezoelectric layers. Aluminum was used to house the acoustic stack. More parameters of the materials used for transducer fabrication are listed in Table II.

The outside surfaces of both plates could be connected to ground while the center electrode between the two plates was connected to the hot wire, as shown in Fig. 4. In this case, the two PZT-2 plates could either be fired together or individually via two BNC cables.

B. Transducer Characterization

Pulse-echo experiment was performed to verify the transducer performance. The transducer was positioned in a tank with degassed water. A steel block was put 15 mm away from the transducer to act as the target. An electrical pulse generated by an Olympus 5077PR square wave pulser/receiver (Panametrics Inc., Waltham, MA) was used to excite the transducer at 100 V. The reflected impulse was first conditioned by the pulser/receiver and then measured and stored by the DSO7104B digital storage oscilloscope (Agilent Technologies Inc., Santa Clara,

CA). The obtained impulse response was then used for determination of sensitivity and bandwidth.

Beam profile and high pressure at focal point were measured with a high-power hydrophone (HNA-0400, Onda Corp., Sunnyvale, CA). In beam profile plotting, a low input voltage of 56 V_{pp} was used to ensure the safety of the hydrophone, considering the long exposure (almost an hour). The input of the transducer was set as bursts of 10 Hz PRF with a 5-cycle sine wave in each burst. The transducer was held in a stable fixture and the hydrophone moved in the emission field to scan the pressure around the focal point. Motion of the hydrophone was controlled by a 3-dimensional stage powered by step motors in each dimension. High pressure at the focal point was measured with increased voltage. Excitation type was the same as previously mentioned, i.e., bursts of 10 Hz PRF with 5-cycle sine wave in each burst. The hydrophone position was adjusted automatically and then fixed at the focal point with increasing voltage through the measurement. In the beam profile measurement, low PRF (10 Hz) and burst with 5-cycle sine wave was also used to excite the transducer to protect the hydrophone from either long-time exposure or very-high-pressure exposure.

C. Tissue Ablation

For hyperthermia ablation, comparison between single-frequency and dual-frequency ultrasound, acoustic power transmitted into tissue should be remained constant. For example, if 6 W was used in tissue ablation, then input power of all frequency combinations was adjusted so that the output acoustic power is 6 W. Power output of the transducer versus the input voltage was calibrated with an ultrasound power meter (UPM-DT-1AV, Ohmic Instruments Co., Easton, MD). A single-channel arbitrary function generator AFG3101 was used to provide waveforms needed, which was amplified by an RF power amplifier Model 3100L (Electronic Navigation Industries Inc., Rochester, NY). Continuous sine waves with different voltages were supplied to the transducer and power was measured by the ultrasound power meter. The amplification of the RF power amplifier is fixed, so voltage of continuous wave was adjusted by the function generator. With the monitor of the ultrasound power meter, voltage needed for each ultrasound type to generate 6 W was recorded, and used later in tissue ablation for comparison.

Tissue ablation tests with the dual-frequency transducer using single-frequency and multi-frequency HIFU were carried out for ablation efficiency comparison. Packaged pork loin tissue was brought to room temperature and left in open air for 30 min before being used for experiments. The tissue was cut to obtain a clean, flat surface from a bulk piece, and then mounted into a 50-mm depth and 150-mm diameter plastic container. Thin steel needles were used to hold the tissue in the designed position relative to the container. The ultrasound transducer was perpendicular to the tissue surface and focused on a certain

depth (e.g., 5 mm) into the tissue sample. A depth of 5 mm was chosen to avoid significant heat dissipation into water. Temperature was measured to numerically indicate the tissue ablation efficiency. A needle thermocouple probe (HYP-0, Omega Engineering Inc., Stamford, CT) with diameter of 0.2 mm was positioned inside tissue at the focal zone to measure the local tissue temperature. A needle thermocouple was chosen to minimize acoustic field interference in tissue. This T-type (Copper-Constantan) thermocouple probe is enclosed in a long hypodermic needle, and also has a fast response with a continuous temperature rating below 200°C. The thermocouple signal was acquired via data acquisition system (USB-6361, National Instruments Corp., Austin, TX) for signal recording and processing.

The porcine tissue sample and HIFU transducers were aligned as described. Ultrasound transducers and the data acquisition system for temperature recording were triggered at the same time. Each measurement consisted of a 45-s ultrasound exposure at 5 mm below the tissue surface. Signals from thermocouple were simultaneously sampled at a rate of 100 samples per second. The output acoustic power of 6 W was introduced for both single- and dual-frequency modes to compare the temperature rises. Each test under the same condition was repeated three times to obtain the average value. The dual-frequency signal was generated by a function generator (AFG3101, Tektronix, Beaverton, OR). The ratios of the amplitudes of each frequency component were 1:1, 1:3, 1:5, and 1:10 (1.5 MHz:3 MHz), and waveforms are shown in Fig. 5. Relative magnitude of the two frequency components could be easily switched from the input waveform.

IV. RESULTS AND DISCUSSION

The final transducer fabricated is shown in Fig. 6. The electrical connection is made by two coaxial cables. The center wires of both cables are connected together to the middle layer of the transducer. The shielding wires of the two cables are connected to the front and back surfaces of the transducer. To excite one layer of the transducer, only one of the cables is connected to power amplifier. To excite both layers, both cables are connected to the power amplifier via a T-shaped connector.

A. KLM Modeling

Electrical impedance and phase spectrum were modeled separately for 1.5 MHz and 3 MHz and the results are shown in Fig. 7. In the modeling result for the 1.5-MHz transducer, one resonance is found at 1.5-MHz. The large aperture of the transducer makes the electrical impedance low. With thin matching layer and no backing layer, the phase at resonance is close to 60°. For the 3-MHz modeling, as predicted, there are two resonant frequencies at

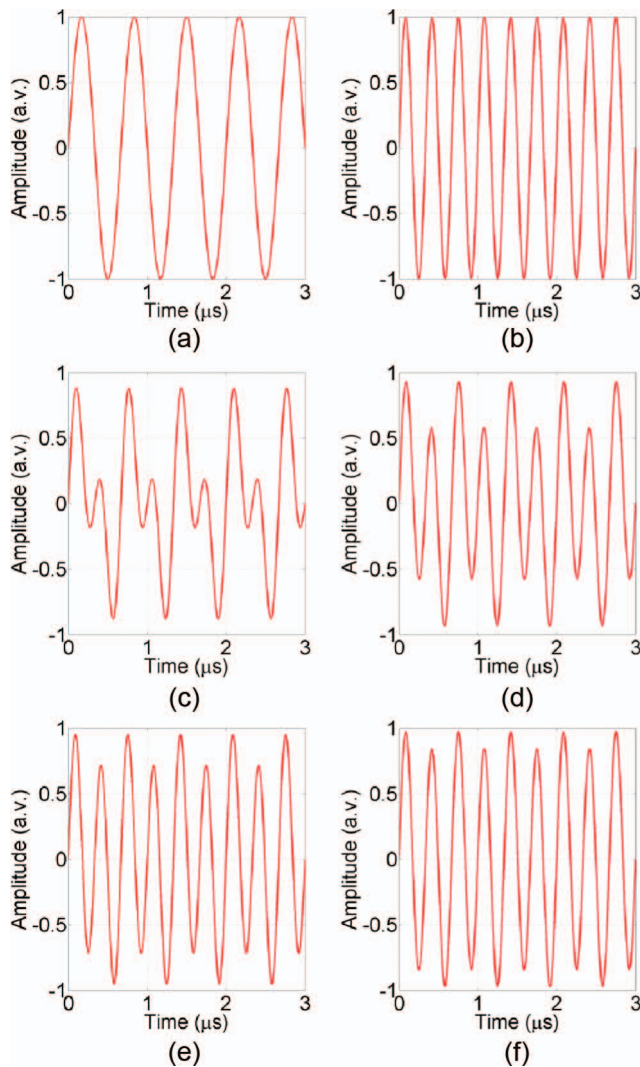


Fig. 5. Signal waveforms generated by the function generator. (a) 1.5 MHz signal, (b) 3 MHz signal, (c)–(f) dual-frequency signals. The ratio of amplitudes between 1.5 MHz and 3 MHz is (c) 1:1, (d) 1:3, (e) 1:5 and (f) 1:10, respectively.

1.5 and 3 MHz, which means the transducer works in two different vibration modes.

The transmitting response was simulated for each frequency with 10-cycle sine wave burst excitation. Driven with the two frequency components, the transducer was expected to generate ultrasound at both frequencies. Based on the modeling, 1.81 and 2.85 kPa/V were expected for 1.5 and 3 MHz ultrasound at the surface of the transducer. The detailed transmitting response is shown in Fig. 8.

B. Pulse-Echo Test

A pulse-echo test was carried out in water tank, with 100 V supplied to the transducer as excitation. A steel block 15 mm away from and facing the transducer acted as the reflection target. The echo signal of the impulse is shown in Fig. 9(a). Ringing of the echo signal is a little bit

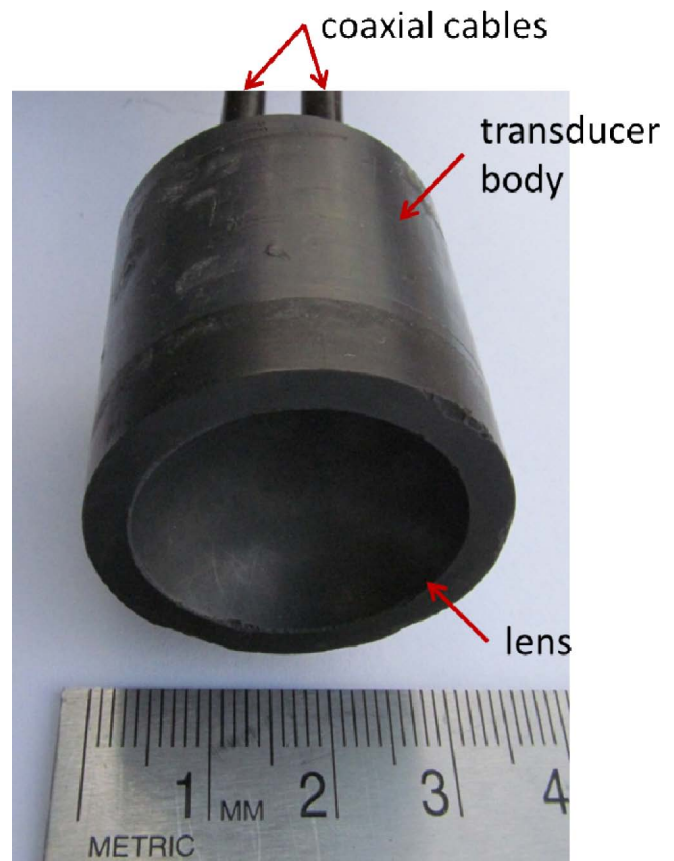


Fig. 6. Photograph of the fabricated dual-frequency transducer.

long because of the light backing and little matching in the transducer. The fast Fourier transform spectrum in Fig. 9(b) clearly shows two strong resonant frequencies at about 1.5 MHz (f_1) and 3 MHz (f_1') with almost identical amplitudes. This directly proved the capability of the transducer for generating 1.5 and 3 MHz ultrasound, and agrees well with the simulation results (Fig. 7). Relative to the base band frequency ($f_1 = 1.5$ MHz), higher order harmonics of the transducer at 4.5 MHz (f_3) and 7.5 MHz (f_5) are very low, with an amplitude of -12.61 dB and -49.29 dB, respectively.

C. Acoustic Pressure

The beam profile of the acoustic field was simulated with Field II and measured with a high-power hydrophone. Simulation results are shown in Figs. 10(a), 10(c), and 10(e). Because of stronger focusing, the 3 MHz ultrasound shows a smaller focal zone than the 1.5 MHz ultrasound. The pressure of 3 MHz ultrasound at focal point is 8.39 MPa, compared with 6.64 MPa for 1.5 MHz ultrasound, corresponding to a power density of 2.35 kW/cm² for 3 MHz ultrasound beam and 1.47 kW/cm² for 1.5 MHz ultrasound beam, respectively. With the same voltage input, the pressure of the dual frequency ultrasound is 8.30 MPa and the power intensity is 1.48 kW/cm². Such power density is high enough to cause cavita-

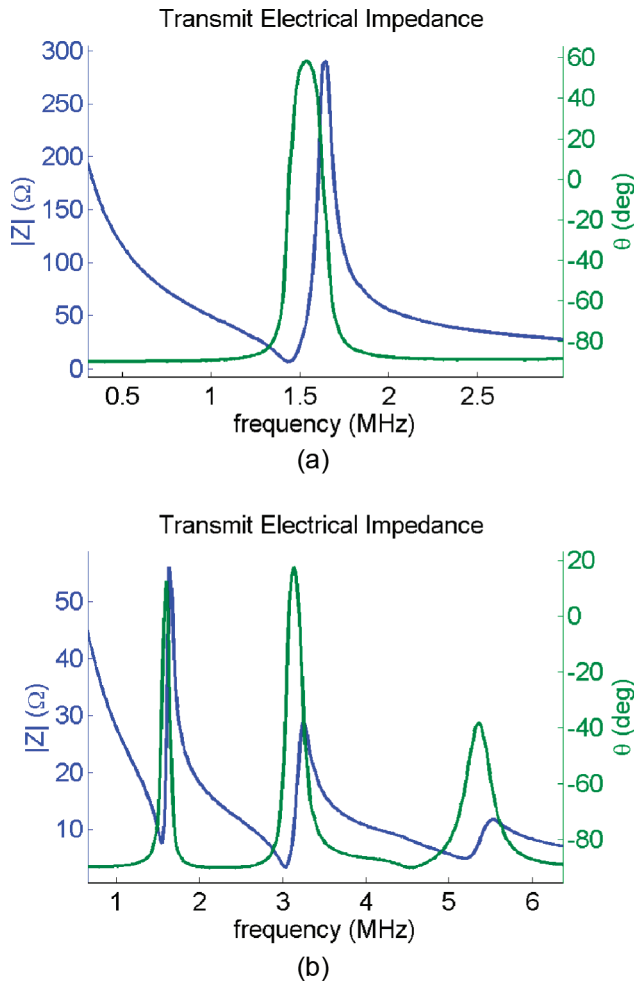


Fig. 7. Impedance and phase of the transducer with (a) dual-layer excitation and (b) front-layer excitation.

tion and hyperthermia effect, thus resulting in lesions in biological tissue [5].

The profile of pressure distribution around the focal point was mapped with hydrophone at 56 Vpp inputs. The results for the scanned field around the focal point are shown in Figs. 10(b), 10(d), and 10(f). As listed in Table III, the beam width and focal depth are much larger than in the simulation. One of the main reasons may be the inaccurate location of the focal point. The focal zone is very sharp (-3 -dB beam width of 0.35 mm for 3 MHz ultrasound), whereas the resolution of mechanical scanning of the water tank system is 0.5 mm. As a result, it is unlikely to measure the exact peak value, and the beam thus seems less focused. The profile of pressure distribution was measured at low pressure with low driving voltages. If driven by high voltage, as used in HIFU application, more nonlinear effect is expected and the beam profile differs slightly [32].

A collection of the beam profile parameters is shown in Table III. Note that the wave of dual-frequency ultrasound is not a sinusoidal wave, and the power density is calculated by integration instead of $P^2/(2Z)$, where P is

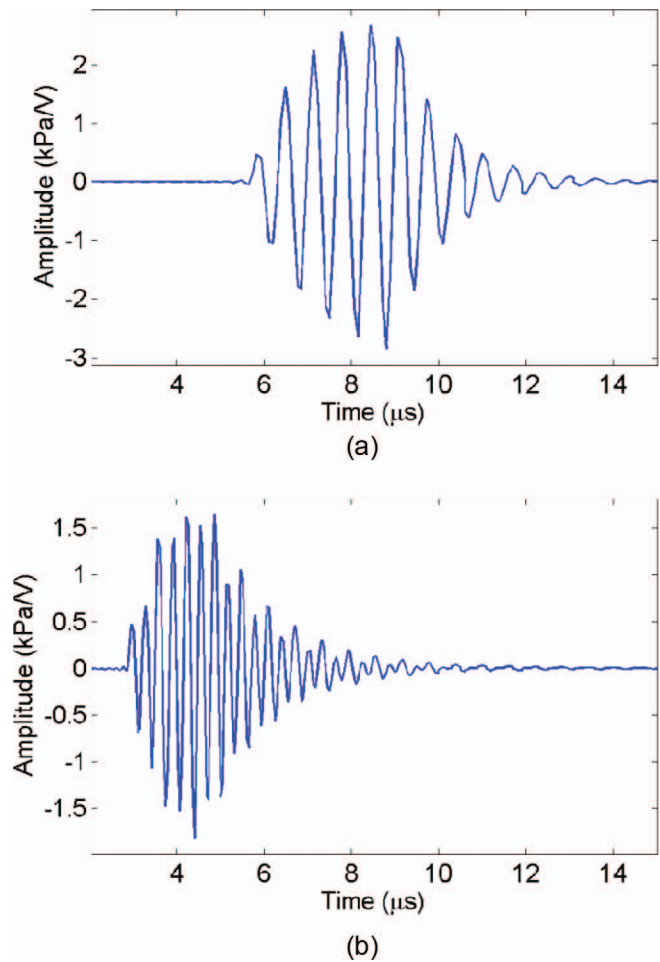


Fig. 8. Acoustic pressure output with 5-cycle burst input at (a) 1.5 MHz and (b) 3 MHz.

the pressure magnitude and Z is the impedance of medium.

Acoustic pressure generated by the transducer at different voltages and frequencies was measured using the high-power hydrophone and the results are shown in Fig. 11. Compared with the simulation, the pressure measured from the hydrophone is lower. Several possible factors may cause this. One factor might be the low scanning resolution as mentioned previously, which will lead to inaccurate positioning of the focal point. Another reason may be imperfection of the transducer lens, causing the less focused effect shown in the beam profile.

D. Tissue Ablation

To make tissue ablation comparison among single-frequency and dual-frequency modes, acoustic power calibration of the transducer at 1.5 MHz, 3 MHz, and dual frequency (1.5 MHz + 3 MHz) was performed to ensure that temperature rise of tissue ablation was compared under the same emitted ultrasound power. An Ohmic ultrasound power meter UPM-DT-1AV was used for the acoustic power measurements. Input voltage was adjusted

TABLE III. BEAM PROFILE OF THE ACOUSTIC FIELD.

Frequency	1.5 MHz	3 MHz	Dual
Simulated			
Focal length (mm)	15	15	15
Peak pressure (MPa)	6.64	8.39	8.30
Peak power density (kW/cm ²)	1.47	2.35	1.48
Beam width (mm)	0.65	0.35	0.45
Focal depth (mm)	2.15	1.1	1.65
Measured			
Focal length (mm)	16.5	15	16.5
Peak pressure (MPa)	2.81	3.64	3.29
Peak power density (kW/cm ²)	0.263	0.442	0.233
Beam width (mm)	2	1.5	1.5
Focal depth (mm)	16.5	9	12.5

Beam width and depth are referred to the -3 dB value.

to generate a given power output. Voltage inputs for an output of 6 W at single frequencies and dual frequency are listed in Table IV. In case of dual-frequency power measurements, the input voltage signal ratio from the function generator of 1.5 MHz to 3 MHz was varied from 1:1 to 1:10 (as shown in Fig. 5) and the required input voltages applied to the transducer were obtained (Table IV).

Under the acoustic power of 6 W at different frequencies, the temperature measurement results are shown in Fig. 12. For porcine tissue ablation, the highest temper-

ature rise was found with dual-frequency ablation with amplitude ratio of 1:10 (1.5 MHz:3 MHz in amplitude). Measurements of each curve were repeated at least 3 times with the same setup and the temperature rise was very consistent, with a variation less than 0.2°C. However, with dual-frequency input, the acoustic pressure distribution is between the two single-frequency experiments (Fig. 11),

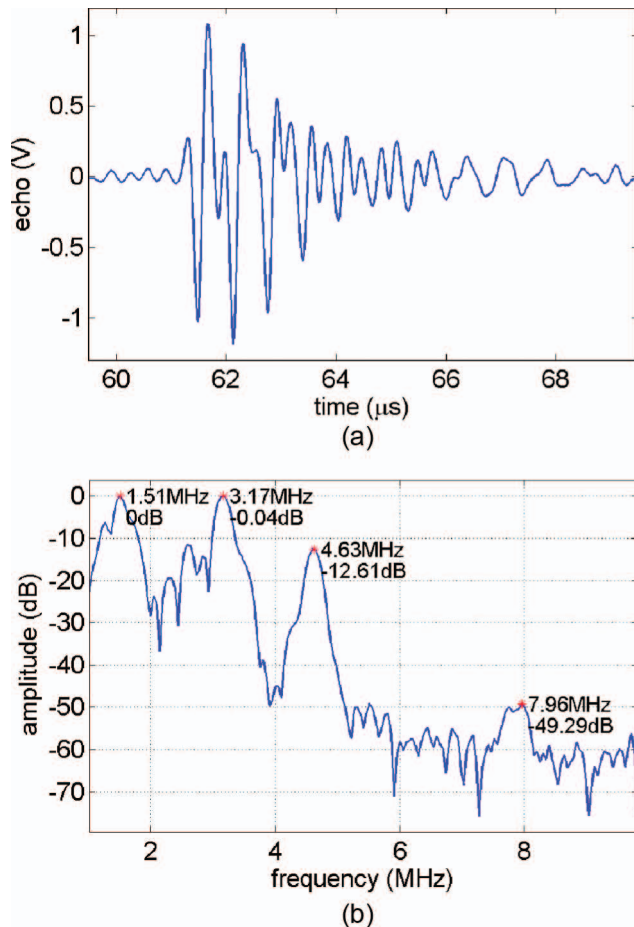


Fig. 9. (a) Reflected waveform and (b) fast Fourier transform of the waveform in pulse-echo test.

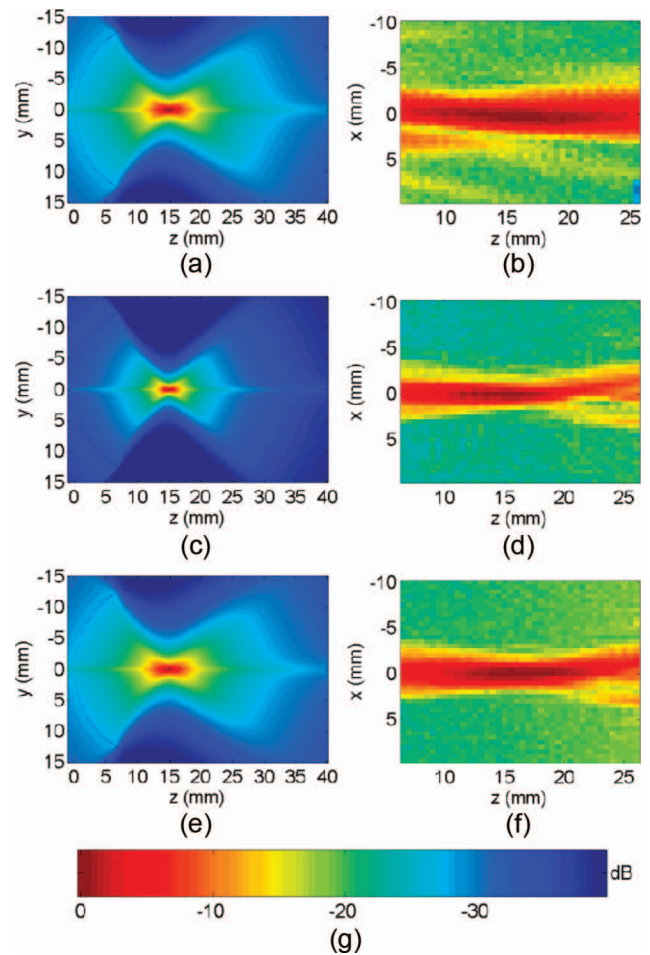


Fig. 10. Ultrasound beam profile with frequency of (a) and (b) 1.5 MHz, (c) and (d) 3 MHz, and (e) and (f) dual frequency. Figures (a), (c) and (e) are from simulation, whereas (b), (d) and (f) are from hydrophone measurement. (g) Color bar is shared by all of the figures.

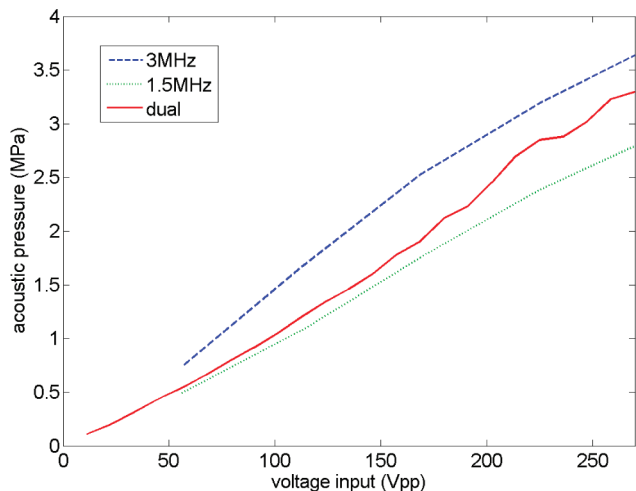


Fig. 11. Acoustic pressure generated by the transducer with different frequency configurations. In this case, the dual frequency means 1.5 MHz and 3 MHz with 1:1 amplitude ratio.

which means that the dual-frequency peak pressure is lower than that of single-frequency 3 MHz ultrasound and higher than that of single-frequency 1.5 MHz ultrasound. Therefore, this finding cannot be explained by the linear bio-heating theory in which tissue temperature rise increases with acoustic pressure in tissue [33].

However, the measured results are similar to previous observations on multi-frequency ablation using different frequencies and tissue materials [14], and larger lesion size was induced by dual-frequency ultrasound than that by single-frequency ultrasound. Dual-frequency ultrasound can generate higher temperatures under the same exposure conditions, which may be attributed to the cavitation yield at different frequencies, even when frequency difference is greater than 500 kHz. The frequency differences in multi-frequency mode may result in a low-frequency homogeneous acoustic wave which will enhance the cavitation effect, according to Iernetti and Feng [34], [35]. A combination of two different frequencies may even result in the formation of constructive and destructive interference patterns that are composed of waves with a wide range of different frequencies and pressure amplitudes. Cavitation is a random frequency-dependent phenomenon, and thus the generation of waves with different frequencies increases the chance of more efficient energy dissipation during cavitation.

TABLE IV. VOLTAGE APPLIED TO THE TRANSDUCER TO GENERATE 6 W OF ACOUSTIC POWER.

Function generator signal	Transducer voltage (V)
1.5 MHz	130
3 MHz	111
1.5 MHz + 3 MHz (1:1)	148
1.5 MHz + 3 MHz (1:3)	128
1.5 MHz + 3 MHz (1:5)	121
1.5 MHz + 3 MHz (1:10)	114

V. CONCLUSION

To achieve high-efficiency HIFU ablation without introducing complexity to system or application, a single-aperture, dual-frequency HIFU transducer was designed, fabricated, and characterized. A pulse-echo experiment showed that the amplitudes of two frequency components are almost equally strong, leading to the advantage that acoustic power output could be easily tuned from the function generator input. Preliminary experiments on tissue ablation showed that higher tissue ablation efficiency can be expected from dual-frequency ablation compared with single-frequency ablation. With proper combination of the two frequency components in the function generator output (e.g., 1:10 in amplitude of 1.5 MHz:3 MHz), but under the same acoustic power output from the transducer, temperature rise measured was consistently more than that induced by single-frequency ultrasound. Specifically, dual-frequency induced temperature rise was more than 100% higher than that generated by single-frequency 1.5 MHz ultrasound, which is mostly attributed to the high-frequency component (3 MHz) used in the dual-frequency ablation. Moreover, dual-frequency-induced temperature rise is 5% higher than that generated by single-frequency 3 MHz ultrasound, which is likely the result of cavitation enhancement by dual-frequency ultrasound. This finding suggests that that dual-frequency HIFU can be an effective approach for more efficient tissue ablation. Further study will focus on exploring ablation volume, optimized amplitude ratio of the two frequencies, phase delay between the two frequencies, and ablation with the guidance of magnetic resonance imaging.

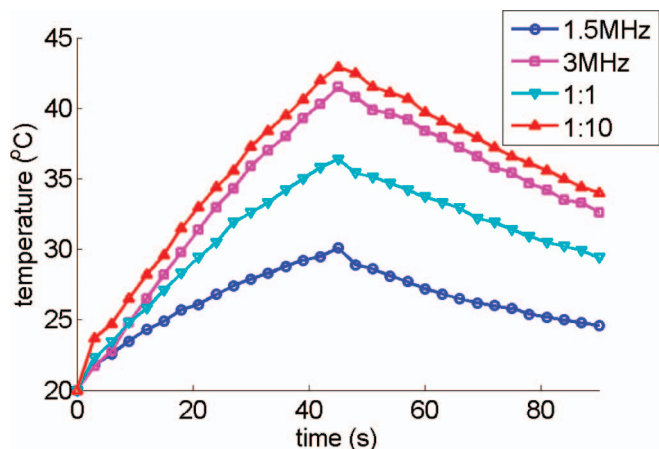


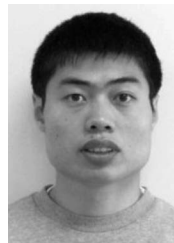
Fig. 12. Porcine tissue ablation tests using single-frequency ultrasound and dual frequency ultrasound with different frequency components under the same power (6 W). In the figure, single frequency ablations are shown with 1.5 MHz and 3 MHz for corresponding frequency. For dual frequency ablations, relative amplitude ratios of 1.5 MHz and 3 MHz are shown as 1:1 and 1:10.

ACKNOWLEDGMENT

The authors thank Dr. W. Lin and Dr. P. Dayton's group at UNC Chapel Hill for the helpful discussions and the help on acoustic field mapping experiments.

REFERENCES

- [1] J. G. Lynn, R. L. Zwemer, A. J. Chick, and A. E. Miller, "A new method for the generation and use of focused ultrasound in experimental biology," *J. Gen. Physiol.*, vol. 26, no. 2, pp. 179–193, 1942.
- [2] W. J. Fry, W. H. Mosberg, J. W. Barnard, and F. J. Fry, "Production of focal destructive lesions in the central nervous system with ultrasound," *J. Neurosurg.*, vol. 11, no. 5, pp. 471–478, 1954.
- [3] Z. B. Wang, F. Wu, Z. L. Wang, Z. Zhang, J. Z. Zou, C. Liu, Y. G. Liu, X. Cheng, Y. H. Du, Z. C. He, M. L. Gu, Z. G. Wang, and R. Feng, "Targeted damage effects of high intensity focused ultrasound (HIFU) on liver tissues of Guizhou Province miniswine," *Ultrason. Sonochem.*, vol. 4, no. 2, pp. 181–182, 1997.
- [4] A. Arefiev, F. Prat, J. Y. Chapelon, J. Tavakkoli, and D. Cathignol, "Ultrasound-induced tissue ablation: Studies on isolated, perfused porcine liver," *Ultrasound Med. Biol.*, vol. 24, no. 7, pp. 1033–1043, 1998.
- [5] J. E. Kennedy, "High intensity focused ultrasound: Surgery of the future?" *Br. J. Radiol.*, vol. 76, no. 909, pp. 590–599, 2003.
- [6] N. McDannold, G. Clement, P. Black, F. Jolesz, and K. Hynynen, "Transcranial MRI-guided focused ultrasound surgery of brain tumors: Initial findings in three patients," *Neurosurgery*, vol. 66, no. 2, pp. 323–332, 2011.
- [7] C. J. Diederich and K. Hynynen, "Ultrasound technology for hyperthermia," *Ultrasound Med. Biol.*, vol. 25, no. 6, pp. 871–887, 1999.
- [8] M. L. Guzman, "The sesquiterpene lactone parthenolide induces apoptosis of human acute myelogenous leukemia stem and progenitor cells," *Blood*, vol. 105, no. 11, pp. 4163–4169, 2005.
- [9] J. E. Kennedy, "High-intensity focused ultrasound in the treatment of solid tumours," *Med. Ultrasound*, vol. 5, no. 4, pp. 1–7, 2005.
- [10] H. Azhari, "Feasibility study of ultrasonic computed tomography-guided high-intensity focused ultrasound," *Ultrasound Med. Biol.*, vol. 38, no. 4, pp. 619–625, 2012.
- [11] F. Marquet, M. Pernot, J. F. Aubry, G. Montaldo, L. Marsac, M. Tanter, and M. Fink, "Non-invasive transcranial ultrasound therapy based on a 3D CT scan: Protocol validation and in vitro results," *Phys. Med. Biol.*, vol. 54, no. 9, pp. 2597–2613, 2009.
- [12] C. D. Herickhoff, G. A. Grant, G. W. Britz, and W. Smith, "Dual-mode IVUS catheter for intracranial image-guided hyperthermia: Feasibility study," *IEEE Trans. Ultrason. Ferroelectr. Freq. Control*, vol. 57, no. 11, pp. 2572–2584, 2010.
- [13] A. Blana, B. Walter, S. Rogenhofer, and W. F. Wieland, "High-intensity focused ultrasound for the treatment of localized prostate cancer: 5-year experience," *Urology*, vol. 63, no. 2, pp. 297–300, 2004.
- [14] P. He, W. Shou, S. Duan, and R. M. Xia, "Dual-frequency high intensity focused ultrasound (HIFU) accelerating therapy," in *27th Annu. Int. Conf. IEEE Engineering in Medicine and Biology Society*, 2005, pp. 213–216.
- [15] P. A. Tatake and A. B. Pandit, "Modelling and experimental investigation into cavity dynamics and cavitation yield: Influence of dual frequency ultrasound sources," *Chem. Eng. Sci.*, vol. 57, no. 22–23, pp. 4987–4995, 2002.
- [16] L. Zhang, H. Zhu, C. Jin, K. Zhou, K. Li, H. Su, W. Chen, J. Bai, and Z. Wang, "High-intensity focused ultrasound (HIFU): effective and safe therapy for hepatocellular carcinoma adjacent to major hepatic veins," *Eur. Radiol.*, vol. 19, no. 2, pp. 437–445, 2009.
- [17] A. Rybyanets, A. Nasedkin, A. Rybyanets, M. Lugovaya, and T. Domashenkina, "Multi-frequency harmonics technique for HIFU tissue treatment," in *IEEE Int. Ultrasonics Symp.*, 2009, pp. 1765–1768.
- [18] G. Iernetti, P. Ciuti, N. V. Dezhkunov, M. Reali, A. Francescutto, and G. K. Johri, "Enhancement of high-frequency acoustic cavitation effects by a low-frequency stimulation," *Ultrason. Sonochem.*, vol. 4, no. 3, pp. 263–268, 1997.
- [19] C. C. Coussios, C. H. Farny, G. Ter Haar, and R. A. Roy, "Role of acoustic cavitation in the delivery and monitoring of cancer treatment by high-intensity focused ultrasound (HIFU)," *Int. J. Hyperthermia*, vol. 23, no. 2, pp. 105–120, 2007.
- [20] C. H. Farny, R. G. Holt, and R. A. Roy, "The correlation between bubble-enhanced HIFU heating and cavitation power," *IEEE Trans Biomed. Eng.*, vol. 57, no. 1, pp. 175–184, 2010.
- [21] L. Carpendo, P. Ciuti, A. Francescutto, G. Iernetti, and G. K. Johri, "Space-time interaction of two ultrasonic fields and sonoluminescence during transient cavitation in distilled water," *Acoust. Lett.*, vol. 11, no. 10, pp. 178–181, 1987.
- [22] R. Feng, Y. Zhao, C. Zhu, and T. J. Mason, "Enhancement of ultrasonic cavitation yield by multi-frequency sonication," *Ultrason. Sonochem.*, vol. 9, no. 5, pp. 231–236, 2002.
- [23] S. Guo, X. Jiang, and W. Lin, "Tissue ablation using multi-frequency focused ultrasound," in *IEEE Int. Ultrasonics Symp.*, 2011, pp. 2177–2180.
- [24] M. Alamolhoda, M. Mokhtari-Dizaji, A. H. Barati, and H. Hasan-zadeh, "Comparing the in vivo sonodynamic effects of dual- and single-frequency ultrasound in breast adenocarcinoma," *J. Med. Ultrason.*, vol. 39, no. 3, pp. 115–125, 2012.
- [25] P. Z. He, R. M. Xia, S. M. Duan, W. D. Shou, and D. C. Qian, "The affection on the tissue lesions of difference frequency in dual-frequency high-intensity focused ultrasound (HIFU)," *Ultrason. Sonochem.*, vol. 13, no. 4, pp. 339–344, 2006.
- [26] R. Chopra, C. Luginbuhl, F. S. Foster, and M. J. Bronskill, "Multi-frequency ultrasound transducers for conformal interstitial thermal therapy," *IEEE Trans. Ultrason. Ferroelectr. Freq. Control*, vol. 50, no. 7, pp. 881–889, 2003.
- [27] R. Krimholtz, D. A. Leedom, and G. L. Mattaei, "New equivalent circuits for elementary piezoelectric transducers," *Electron. Lett.*, vol. 6, no. 13, pp. 398–399, 1970.
- [28] J. A. Jensen, "Calculation of pressure fields from arbitrarily shaped, apodized, and excited ultrasound transducers," *IEEE Trans. Ultrason. Ferroelectr. Freq. Control*, vol. 39, no. 2, pp. 262–267, 1992.
- [29] C. Wang, J. Li, and M. Zhao, *Piezoelectric & Ferroelectric Physical*. Beijing, China: Science Press, 2009.
- [30] A. W. Lawson, "The vibration of piezoelectric plates," *Phys. Rev.*, vol. 62, no. 1–2, pp. 71–76, 1942.
- [31] G. R. Lockwood and F. S. Foster, "Modeling and optimization of high-frequency ultrasound transducers," *IEEE Trans. Ultrason. Ferroelectr. Freq. Control*, vol. 41, no. 2, pp. 225–230, 1994.
- [32] M. R. Bailey, J. A. Reed, B. W. Cunitz, P. J. Kaczowski, and L. A. Crum, "Effects of nonlinear propagation, cavitation, and boiling in lesion formation by high intensity focused ultrasound in a gel phantom," *J. Acoust. Soc. Am.*, vol. 119, no. 3, pp. 1834–1848, 2005.
- [33] G. T. Haar and C. Coussios, "High intensity focused ultrasound: Physical principles and devices," *Int. J. Hyperthermia*, vol. 23, no. 2, pp. 89–104, 2007.
- [34] G. Iernetti, P. Ciuti, N. V. Dezhkunov, M. Reali, and A. Francescutto, "Enhancement of high-frequency acoustic cavitation effects by a low-frequency stimulation," *Ultrason. Sonochem.*, vol. 4, pp. 263–268, Jul. 1997.
- [35] R. Feng, Y. Y. Zhao, C. P. Zhu, and T. J. Mason, "Enhancement of ultrasonic cavitation yield by multi-frequency sonication," *Ultrason. Sonochem.*, vol. 9, pp. 231–236, Oct. 2002.

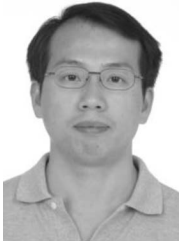


Jianguo Ma received his B.S. degree in 2008 and his M.S. degree in 2011, both from the School of Physics, Shandong University, China. He has been working on his Ph.D. research in the Department of Mechanical and Aerospace Engineering at North Carolina State University since 2011. Currently, he is Dr. Xiaoning Jiang's student, working at the Micro/Nano Engineering Laboratory. His main research interests are piezoelectric ultrasound transducer design and fabrication.



Sijia Guo received his B.S. degree from the Department of Mechanical Engineering at Zhejiang University (ZJU), China, in 2009. Currently, he is a Ph.D. student in the department of Mechanical and Aerospace Engineering at North Carolina State University, Raleigh, NC. His main research interests are applications of ultrasound, ultrasonic transducer design, and acoustic field modeling.

From 1983 to 1986, he was an engineer at The Center of Microelectronics, Chinese Academy of Sciences, Beijing, China. His work focused on the computer-aided design of integrated circuits and the modeling of the IC process. From 1990 to 1993, as a research assistant at the ultrasonic lab of the Institute of Acoustics, he worked on nondestructive testing of materials, acoustic wave logging, and design, fabrication, and characterization of 1-3 piezocomposites for ultrasonic transducer applications. Since 1998, as a senior scientist at Blatek Inc., he has focused his effort on ultrasonic transducer design for medical and industrial applications.



Di Wu received his Ph.D. degree from the Institute of Acoustics, Chinese Academy of Sciences, China. In 2007, he started his work as a lecturer in the College of Sciences at Beijing Jiaotong University. Currently, he is working as a visiting scholar at the Micro/Nano Engineer Laboratory of North Carolina State University under Dr. Jiang. His main research interests are ultrasonic transducers and ultrasonic nondestructive testing.



Xiaoning Jiang received his Ph.D. degree from Tsinghua University in 1997 and postdoctoral training from Nanyang Technological University and The Pennsylvania State University (from 1997 to 2001). He worked in industry (Standard MEMS Inc. and TRS Technologies Inc.) before joining North Carolina State University in 2009 as an Associate Professor of Mechanical and Aerospace Engineering. Dr. Jiang is the author or co-author of two book chapters, one book, six issued U.S. patents and more than 10 U.S. patent applications,

and more than 50 technical papers and presentations on piezoelectric composite micromachined ultrasound transducers (PC-MUT), ultrasound for medical imaging and NDE, smart materials and structures, and M/NEMS.

Xuechang Geng received a B.S. degree in physics from Xi'an Jiaotong University, Xi'an, China, in 1983; an M.S. degree in acoustics from The Institute of Acoustics, Chinese Academy of Sciences, Beijing, China, in 1989; and a Ph.D. degree in material engineering from The Pennsylvania State University in 1997.